Progress In Electromagnetics Research C, Vol. 118, 147–158, 2022

Vernier Effect Based Temperature Sensor Revealed Ultra-Sensitivity with High-Detection Resolution

Lashari G. Abbas[1], Farhan Mumtaz[1, 2, 3, *], Yutang Dai[1, *],
Rashda Parveen[3], and Muhammad A. Ashraf[3]

Abstract—In this study, a Vernier effect based temperature sensor with ultra-sensitivity and high-resolution detection is presented. The structure of the proposed temperature sensor is based on dual cascaded Fabry-Perot interferometers (FPIs), which consists of polymer and air cavity FPIs. The polymer cavity works as the sensing part, whereas the air cavity works as the reference part. The slight difference between the Free Spectral Range (FSR) of the sensing and the reference FPIs can establish the Vernier effect, which improves the sensitivity of the cascaded FPIs structure compared to the single FPI structure. The experimental results show that the proposed structure can provide the ultra-high temperature sensitivity of 67.69 nm/°C that is 20 times higher than the single FPI, which is 3.36 nm/°C in the testing range of 26°C–28°C. In addition, the structure is simple to fabricate, compact, inexpensive, along with ultra-sensitivity and high-resolution. Therefore, the proposed sensor is a suitable choice for the applications demanding high resolution temperature detection in different fields of engineering and science.

1. INTRODUCTION

Of the many physical parameters measured in an environment, temperature is considered to be the most measured parameter. In the day-to-day activities of human life, temperature parameter is directly or indirectly linked to the many physical parameters. To detect minor variations in temperature, a high-resolution sensing device is required. Precise temperature measuring instruments are gaining prominence in almost every major field of engineering and science, including nuclear tests, chemical reactions, biotechnology, etc. However, their demand for ultra-high sensitivity and ultra-low tracing range is also evolving in remote and artificial intelligence systems. Since the conceptual implementation of fiber optic sensors, they have demonstrated their invincible advantages, namely high sensitivity, compact design, light weight, immunity to electromagnetic interference, and many other capabilities.

Over the past decade, numerous optical fiber-based temperature sensing architectures have been developed. Mach Zehnder Interferometers (MZIs) [1–4], Sagnac Interferometers [5–8], Fabry-Perot interference (FPI) Sensors [9–12], Surface Plasmon Resonance (SPR) Sensors [13–17], Silicon On Insulator (SOI) sensor [18], Fiber Bragg Gratings (FBGs) Sensor [19–21], and Long-Period Fiber Gratings (LPFGs) [22–24] are popular in temperature measuring devices. Most interferometers, including conventional FBGs, are shown to have low-temperature sensitivities due to the low thermal-optical coefficient (TOC) and thermal-expansion coefficient (TEC) of silica. Although SPR sensors are found as ultra-sensitive temperature devices, their structures involve expensive materials for manufacturing. SOI sensors have also shown high sensitivities to temperature because of high TOC

Received 24 December 2021, Accepted 9 February 2022, Scheduled 19 February 2022

* Corresponding author: Farhan Mumtaz (mfmawan@mst.edu; mfmawan@yahoo.com), Yutang Dai (daiyt6688@whut.edu.cn).

[1] National Engineering Laboratory for Fiber Optic Sensing Technology, Wuhan University of Technology, Luoshi Road 122#, Wuhan 430070, China. [2] Department of Electrical and Computer Engineering, Missouri University of Science and Technology, Rolla, MO 65409, USA. [3] Department of Electronics, Quaid-i-Azam University, Islamabad 45320, Pakistan.

and TEC of silicon, but several fabrication constraints are observed, i.e., coupling of silicon with fiber or else. Various methods have been reported for the manufacturing of temperature sensors, i.e., core misaligned [25], micro-machining by femtosecond laser [26], in-filtration of photonic crystal fibers [27, 28], micro/nano-tapering of fiber [2, 29], etc. However, these sensors can produce temperature sensitivities up to a few tens or hundreds of pm/°C.

In modern times, Vernier effect-based sensors are gaining popularity due to their ultra-sensitive response. Their concept of actualization can be deduced from the superimposition of two or more interferometers spectra, which are integrated with each other in the formation of cascades or else. Due to the slight difference in their sensing length, each length presents a different and unequal Free Spectral Range (FSR). As a result, it contributes to the superimposition of the obtained spectrum and enhances the detection and resolution of sensors. Different research groups have studied Vernier effect based sensors, which mainly include cascaded FPIs sensors [30, 31], cascaded Sagnac loop sensors [32, 33], Sagnac with FPI [34], MZI in-line sensors [35, 36], hybrid MI and FPI [37], etc. In contrast to the FPIs and Sagnac, the Vernier effect in MZIs is rarely used to enhance sensitivity, as MZIs exhibit irregular and intermittent interference patterns. However, FPIs have shown outstanding performance in temperature sensing, where the preparation of dual FPI in a single interferometer is the best way to increase the sensitivity, as well as the resolution range via the Vernier effect. In temperature measuring FPIs, a single FPI holds low sensitivity, while dual FPIs with the Vernier effect is appealing to enhance the temperature sensitivity. Besides, extrinsic FPIs [38, 39] illustrated in-sensitive response to the refractive index along with several advantages of easy manufacturing, compact size, etc. Therefore, from the literature discussed above, it can be inferred that FPI itself is a good candidate for independent detection of temperature change and could easily maintain single parameter of temperature sensing. However, traditional FPIs with low TOC and TEC exhibit considerably low sensitivity, whereas the replacement of cavity with high TOC and TEC materials could easily improve the sensor's sensitivity [12].

In order to improve the temperature sensitivity, an ultra-sensitive and high-resolution temperature sensor of a dual cascaded FPIs structure is demonstrated in this paper. The proposed sensor can easily produce a Vernier effect, which improves the temperature sensitivity up to 20× times compared to a single FPI structure. One of the FPIs — cavity comprises NOA65 polymer, which is taken as sensing interferometer and is used as a substitute for low to high TOC and TEC characteristics. Another FPI — cavity is made up of HCF and is taken as a reference interferometer. Due to low TOC of air, the sensitivity of reference FPI is relatively low, with no need to isolate it from sensing FPI, which was reported earlier [32]. A temperature resolution of 2.95×10^{-4} and 5.95×10^{-3} is obtained for dual cascaded and single FPIs, respectively. The main features of the proposed structure are ultra-high sensitivity, high resolution detection, simple fabrication, and low cost. Therefore, the proposed sensor is a suitable choice for various industrial applications demanding high resolution temperature detection.

The rest of the paper is organized as follows. In Section 2, material parameters, fabrication, and theoretical analysis of the proposed sensor are discussed, whereas experimental results and discussion with respect to the Vernier effect are demonstrated in Section 3.

2. FABRICATION AND WORKING PRINCIPLE

2.1. Material Parameters

The schematic representation of the proposed dual cascaded FPI temperature sensing device is illustrated in Figure 1(a). It consists of SMFs (SMF1 SMF2 and SMF3), adhesive thermos-sensitive polymer NOA65, and HCF. The FPI's micrographs are recorded by a microscope, as shown in Figures 1(b)–(c). SMF (corning-28) has a core and clad diameter of 8.2 μm and 125 μm, respectively. NOA65 adhesive polymer is in transparent form. Initially, it is a liquid photopolymer that can be easily converted into solid form when it is exposed to Ultraviolet (UV) light. The refractive index of the solid NOA65 polymer is 1.52. HCF consists of a large air hole, and its hole and clad diameters are 62 μm and 125 μm.

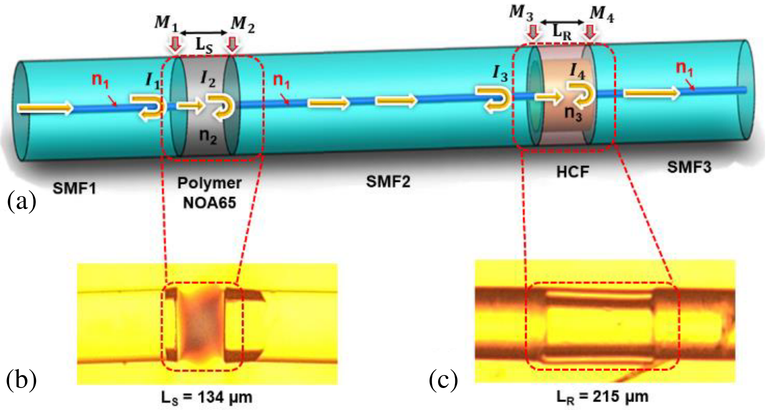

Figure 1. (a) Schematic diagram of the temperature sensor with dual cascaded FPIs; and (b) its longitudinal cross-section under the microscope consist of NOA65 adhesive polymer ($L_S = 134\,\mu\text{m}$) for sensing FPI, and (c) HCF ($L_R = 134\,\mu\text{m}$) cavity for reference FPI.

2.2. Sensor Fabrication

The proposed FPI sensor is designed with a simple technique of cleaving, aligning, and UV curing. The preparation of the sensor involves the following steps: Step-1, SMF1, and SMF2 are cleaved with the help of a high precision cleaver, as shown in Figure 2(a). Step-2, the cleaved end facets of the SMF1 and the SMF2 are immersed into the NOA65 adhesive polymer (liquid form) for about 30 seconds approximately, and then this adhesive polymer would easily attach to the end facets of each SMF that is a cause of capillary action, as shown in Figure 2(b). Step-3, SMF1 and SMF2 are placed on a fusion splicing machine, where NOA65 is attached on their end facets tips. The manual mode of the splicer is used to align so that NOA65 adhesive polymer can be attached, and the desired distance between SMF1 and SMF2 can be achieved. Then, NOA65 adhesive polymer is dried by exposing it to UV light for about 30 minutes, as shown in Figure 2(c). As a result, the NOA65 turned into a solid transparent photopolymer and formed a polymer FPI sensing cavity. Since NOA65 is in the form of transparent polymer, and it can be easily converted from liquid photopolymer state to solid-state, when UV light of wavelength range from 350 nm to 380 nm is exposed on it. The UV point source light of type UV LED light curing equipment (FUV-6BK) is used for the manufacturing of the NOA65 polymer-based FPI cavity. Step-4, afterward, the creation of reference FPI cavity is scheduled which is constituted via a simple process of fusion splicing. However, the fabrication process of the reference FPI is simpler than that of the sensing FPI. Firstly, a piece of SMF3 is cleaved and spliced with one end facet of HCF, then the other end facet of the same HCF is cleaved at a desired cavity length of L_R and spliced with another SMF to form an interference cavity termed as reference FPI cavity. Step-5, the two cavities are then joined together in a back-to-back formation, called a cascaded FPI structure, as shown in Figure 2(d). The interference of two cascaded FPIs magnifies the reflection spectrum due to the Vernier effect, which enhances the temperature sensitivity of the proposed sensing device.

2.3. Theoretical Analysis

To achieve the Vernier effect phenomenon, dual cascaded FPIs are constituted, and the input light is excited from SMF1 that passes through NOA65 polymer cavity. As a result, Fresnel reflection occurs at the mirror (M_1). However, a portion of light reflects while the remaining light propagates through the NOA65 polymer. When the light reaches the mirror (M_2), again a portion of light reflects and transmits. Similarly, this sequence of transmission and reflection follows at reference FPI of mirror (M_3) and mirror (M_4). On the whole, four beams of light are reflected from four different mirrors, i.e., M_1, M_2, M_3, and M_4. Thus, by combining these mirrors light intensities for dual cascaded FPIs, the

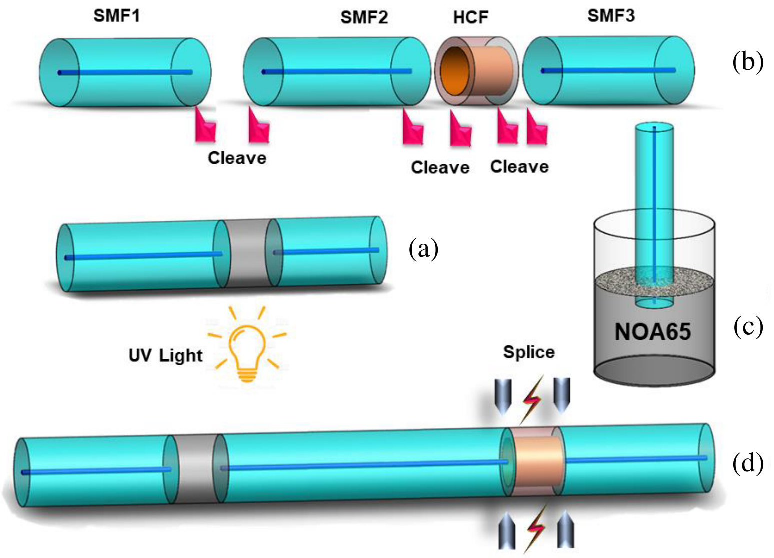

Figure 2. Fabrication steps of the temperature sensor with dual cascaded FPIs.

total light intensity of reflection at receiving side can be expressed as,

$$I = I_1 + I_2 + I_3 + I_4 + 2\sqrt{I_1 I_2}\cos(\theta_S) + 2\sqrt{I_3 I_4}\cos(\theta_R) \tag{1}$$

where I_1, I_2, I_3, and I_4 are the light intensities reflected by the four reflective surfaces, called mirrors: M_1, M_2, M_3, and M_4, respectively. θ_S and θ_R are cosine angles between two different reflected light signals of sensing and reference FPIs, respectively. To generate the Vernier effect, the optical paths of two FPIs need to be very close to each other but not equal. It can be realized by making the lengths of the two FPI cavities slightly different. Thus, the cavity length of any FPI can be calculated as,

$$L = \frac{\lambda_m \lambda_{m+1}}{2n_{\mathit{eff}}\left(\lambda_m - \lambda_{m+1}\right)} \tag{2}$$

where n_{eff} is the effective refractive index for the sensing (n_2) or reference (n_3) cavity, and L is the length of the cavity. λ_m, λ_{m+1} are the adjacent dips (or peaks) of wavelengths in the reflection spectrum/interference pattern. The formulation scheme of the proposed sensor is divided into two parts. First, the temperature sensitivity of a single FPI is analyzed, including a sensing structure (NOA65). The structure of sensing FPI consists of SMFs and NOA65 polymer, as shown in Figure 1. Sensing FPI cavity length is L_S, and it is different from the change in length ΔL_S, thus wavelength λ_m of m-th interference peak can be estimated as,

$$\lambda_m = \frac{4\pi n_2(\Delta L_s)}{2m+1} \tag{3}$$

Here, the cavity formed in the sensing FPI is part of the thermos-sensitive polymer (NOA65). When the temperature variation occurs, NOA65 polymer fills in between the SMFs expands. As a result, a sufficient change in the cavity length of NOA65 polymer is predicted due to high TEC and TOC. Thus, the corresponding wavelength shift is caused by the temperature change, which can be expressed as.

$$\delta\lambda_m = \frac{\partial\lambda}{\partial T} = \lambda^m_{dip}\left(\alpha + \xi\right), \quad m = 0, 1, 2, \ldots \tag{4}$$

where α and ξ are the TEC and TOC, respectively. TEC and TOC can be mathematically expressed as

$$\alpha = \left(\frac{1}{n_2} \cdot \frac{dn_2}{T}\right) \tag{5}$$

$$\xi = \left(\frac{1}{L} \cdot \frac{dL}{T}\right) \tag{6}$$

However, those structures composed of all-fiber FPI cavities possess low-temperature sensitivities compared to that of NOA65 polymer cavities, which is due to the low TEC and TOC of the silica material. Highly thermos-sensitive material for designing of sensing FPI cavity is an excellent candidate that helps to enhance temperature sensitivity drastically. Keeping in mind the use of thermo-sensitive material, the proposed FPI sensor is designed to demonstrate an ultra-sensitive structure for temperature measurement, featuring high TEC and TOC polymer.

In order to further improve the temperature sensitivity, the sensing FPI is cascaded with reference FPI to generate a Vernier effect. Vernier effect appears when the Free Spectral Range (FSR) of the reference FPI is very close to that of the sensing FPI. Generally, the difference between the FSRs of the two FPIs is about one tenth of their FSRs. Slight difference between FSR of sensing and reference FPIs produces the Vernier effect. Theory of FSR explains that the FSR for reference and sensing FPIs can be achieved as,

$$FSR_R = \lambda_R(m-1) - \lambda_R(m) = \frac{\lambda_R^2}{2n_3 L_R} \tag{7}$$

$$FSR_S = \lambda_S(k-1) - \lambda_S(k) = \frac{\lambda_S^2}{2n_2 L_S} \tag{8}$$

The above equations show that the FSR of the sensing cavity and reference cavity depends on the lengths and refractive indexes of the two cavities. The refractive index of the sensing (polymer) cavity and reference (air) cavity is 1.52 and 1.0, respectively. The lengths and FSRs of the two cavities are given in Table 1. Further, FSR_R and FSR_S can be combined to produce a FSR_{env} that can be defined as,

$$FSR_{env} = \frac{FSR_R \times FSR_S}{|FSR_R - FSR_S|} \tag{9}$$

The envelope of the spectrum is formed in the favour of Vernier effect, which greatly improves temperature sensitivity through tracing of envelope shifts in the reflection spectrum of the proposed sensor. The magnification factor M is the number that predicts the sensitivity, which is M times of sensing FPI sensitivity. In the response to the Vernier effect, M can be calculated as,

$$M = \frac{FSR_S}{FSR_R - FSR_S} \tag{10}$$

where the wavelength shift of the envelope can be expressed as

$$\begin{aligned} \delta\lambda_{env} &= \delta\lambda \times M \\ \delta\lambda_{env} &= \frac{FSR_S}{FSR_R - FSR_S} \times \lambda_{dip}^m (\alpha + \xi) \quad ; \quad m = 0, 1, 2, \ldots \end{aligned} \tag{11}$$

where $\delta\lambda$ is the resonant wavelength that shifts with the temperature variation of a single FPI-based sensor; M represents the magnification factor, which is directly related to the optical lengths of sensing-FPI and reference-FPI. L_S and L_R are predicted from Eq. (6) and Eq. (7), which are corresponding to optical cavity lengths of the sensing and reference FPIs, respectively. From Eq. (9), it can be estimated from the change of envelope $\delta\lambda_{env}$ that the wavelength of dual FPIs shifts M times of sensing FPI.

3. EXPERIMENTAL RESULTS AND DISCUSSIONS

3.1. Independent Test of Reference FPI and Sensing FPI

The schematic testing setup for temperature measurement is shown in Figure 3. An Amplified Spontaneous Emission (ASE) source with a resonant wavelength of 1550 nm is used to inject the light through SMF lead-in to the sensor. The reflected beam of light is recombined using an optical coupler (OC), and the reflection spectrum is monitored using an Optical Spectrum Analyzer (OSA). The wavelength resolution of the OSA is set to 0.02 nm. In order to observe a distinct spectrum of the Vernier effect, two FPIs of cavity length are prepared, i.e., sensing FPI ($L_S \approx 134\,\mu\text{m}$) and reference FPI ($L_R \approx 215\,\mu\text{m}$). Initially, a single FPI cavity consisting of NOA65 adhesive polymer is tested for sensing performance and conforms to the physical optical length of the cavity. Figure 4 shows the reflection

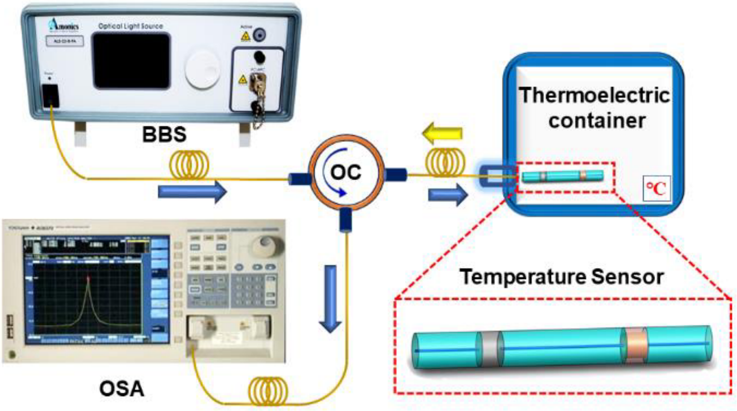

Figure 3. Experimental setup for temperature measurement.

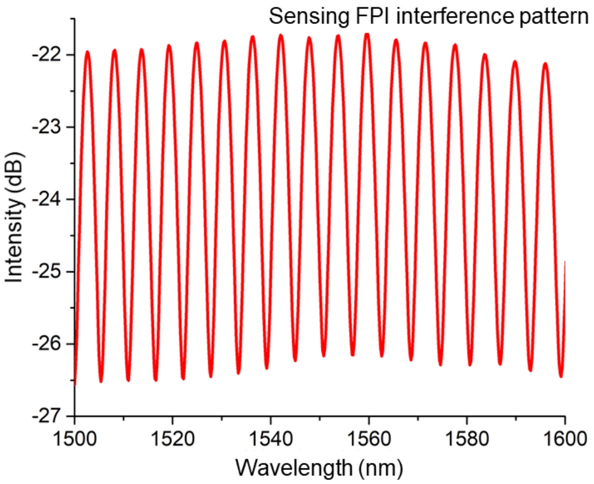

Figure 4. Interference spectrum of single sensing FPI where cavity consists of NOA65 thermo-sensitive polymer.

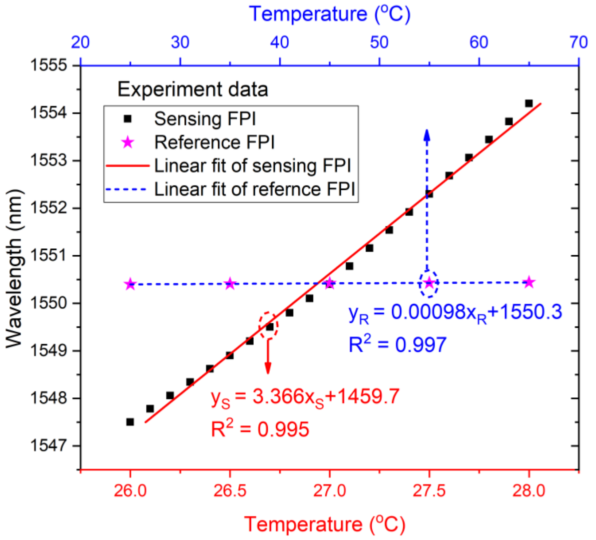

Figure 5. Sensitivity and linear correlation response of temperature sensors: single sensing FPI is shown in red line while single reference FPI is shown in blue dotted line.

spectrum of sensing FPI with cavity length L_S. Before proceeding to investigate the performance of dual cascaded FPIs together, independent testing for sensing FPI and reference FPI is taken into account. Firstly, sensing FPI is placed into a thermoelectric container with a resolution of 0.01°C. Besides, a thermometer probe is also inserted into the thermoelectric container to refine the error. The output spectra of sensing FPI ranging from 26°C to 28°C are obtained with a temperature shift step of 0.1°C. The spectral evolution of sensing FPI exhibits a temperature sensitivity of 3.36 nm/°C, which is as expected similar to results of the earlier reported single FPI temperature sensor composed of NOA65 adhesive polymer [12]. However, the same procedure is repeated for reference FPI consisting of HCF and obtains temperature sensitivity of 0.98 pm/°C in the range of 25°C–65°C, which is also similar as expected. It can be conferred from the results that sensing FPI has produced a large shift in wavelength, while reference FPI has hardly changed. Linear correlation fitting of sensing and reference FPIs along with their sensitivities is shown Figure 5, and their interference shift with temperature rise can be seen in Figures 6(a)–(b), respectively.

To demonstrate the Vernier effect response of dual cascaded FPIs temperature sensor, the sensor is placed into a thermo-electric container, whose temperature measurement error is about 0.01C.

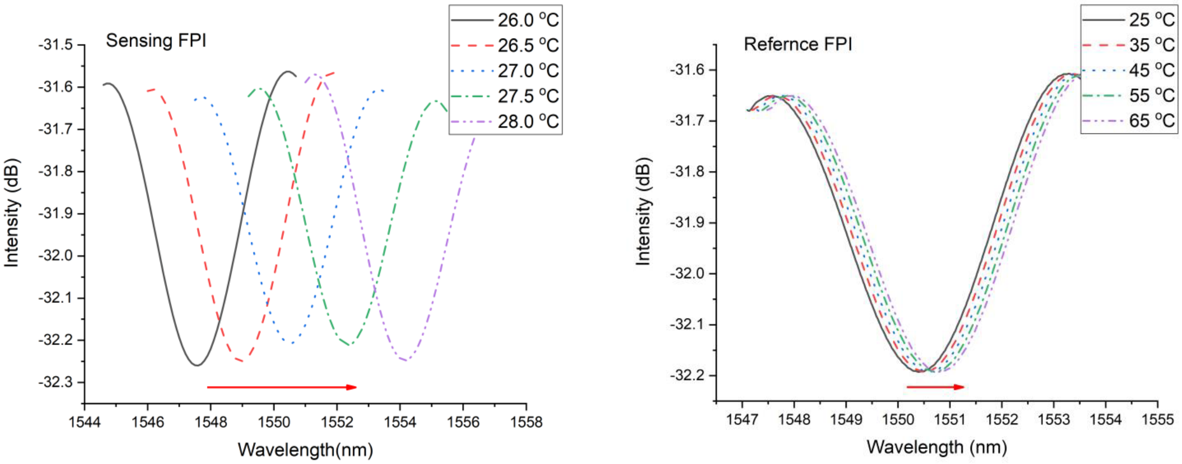

(a) (b)

Figure 6. Spectral evolutions of (a) sensing FPI response, and (b) reference FPI response.

3.2. Veriner Effect Test of Dual Cascaded FPIs

To demonstrate the Vernier effect response of dual cascaded FPIs temperature sensor, the sensor placed into a thermo-electric container, whose temperature measurement error is about 0.01°C. The experimental investigations for dual FPIs have also proceeded with the same experimental setup as shown in Figure 3. The interference spectrum consisting of an upper envelope and a lower envelope superimposed on a comb-like fringes pattern, as shown in Figure 7. Vernier effect spectrum gives two large fringes which are spread over a long-wavelength spectral range of 1450 nm–1650 nm. Both of the Vernier effect fringes from Upper and lower envelopes are so obvious and equally contributed, which are shown in the red and blue lines. Temperature measurements are taken in the range of 26°C–28°C with an increasing step of 0.1°C.

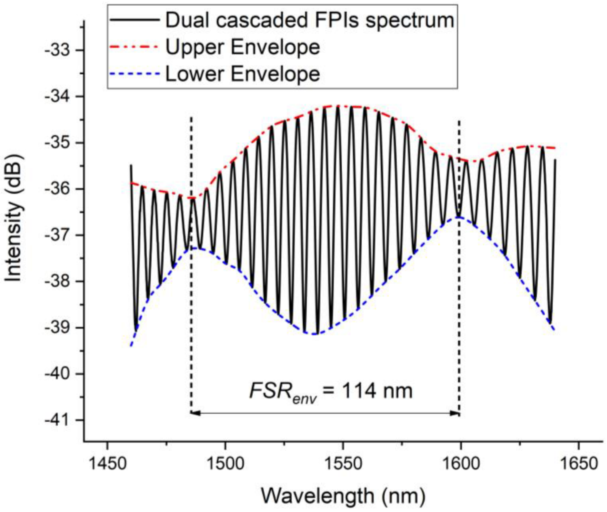

Figure 7. Interference spectrum of dual cascaded FPIs of the temperature sensor.

Fringes envelope is too large in size and produces large FSR, and resultantly, temperature measurements cannot exceed 28°C due to source power and bandwidth limitations. The fringe shift response of the dual cascaded FPIs can be seen in Figure 8, and inset shows that the temperature has

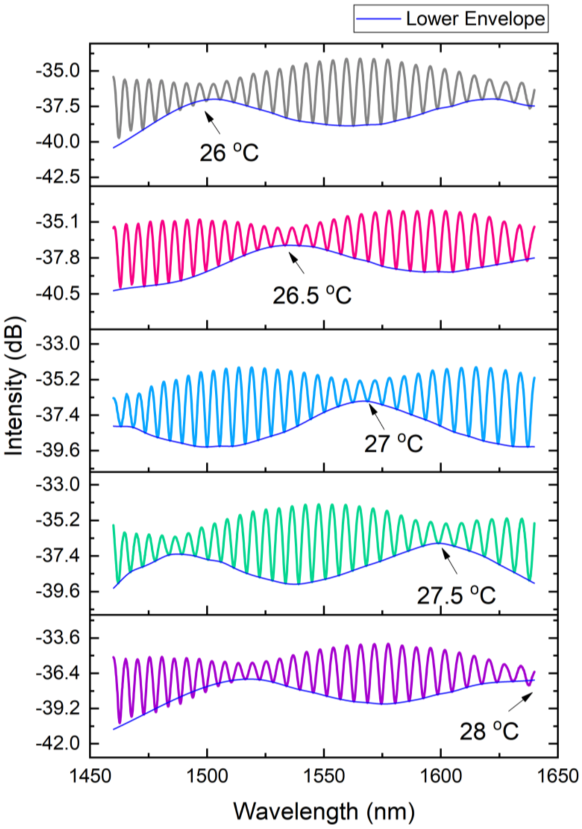

Figure 8. Spectral evolutions of the proposed temperature sensor with dual cascaded FPIs.

increased by 0.5°C. The spectrum shows that the sensor produces a red-shift with the temperature rise. Further, linear regression method is employed to obtain the sensitivity and linear fitting line of the sensor, as shown in Figure 9. The sensor with dual cascaded FPIs exhibits ultra-temperature sensitivity of 67.69 nm/C with a high linear correlation value of 0.99924, which is remarkable and 20× times higher than that of a single FPI sensor. From Eq. (9), it is theoretically forecasted that magnification factor $M \approx 18.99$, with FSRs ($FSR_{Sensing} \approx 5.89\,\text{nm}$, and $FSR_{Reference} \approx 5.58\,\text{nm}$) is consistent with the experimentally obtained value of $M = 20.14$. Both single FPI and dual cascaded FPIs show positive values in spectral wavelength, which is due to the expansion of sensing cavity length ΔL_S and optical path difference of cavities $\Delta|L_S - L_R|$ with temperature rise, respectively. As theory explains when $L_S < L_R$, ΔL_S and $\Delta|L_S - L_R|$ can have positive or negative values depending on the reaction of the spectrum and the envelope with an increase or decrease in temperature, respectively. Experimental results are highly consistent with theoretical analysis as expected, which confirms the accuracy and feasibility of the sensor. In addition, the sensitivity factor can be arbitrarily designed and controlled by adjusting the cavity lengths, as explained in theory. The proposed ultra-sensitive temperature device has shown extraordinary performance during the experiment, and its key parameters along with sensitivities are listed in Table 1.

Table 1. Parameters and sensitivity of FPIs.

FPI type	**Cavity "L (μm)"**	**FSR (nm)**	**Sensitivity (nm/°C)**
Dual FPIs	$L_S = 134$, $L_R = 215$	114 ($FSR_{envelope}$)	67.693
sensing FPI	134	5.89	3.36
reference FPI	215	5.58	0.00098

A comparison is made with recently reported temperature sensors, which is listed in Table 2. The proposed sensor is an ultra-sensitive and high-resolution temperature device. Based on its performance and simple structure, it can be a suitable candidate for various practical applications in medicine and engineering.

Table 2. Comparison of the proposed sensor.

Ref.	Sensor structure	Vernier effect	Sensitivity
[3]	Etched multicore fiber-MZI	No	66.73 pm/°C
[4]	Ellipsoidal balls MZI	No	136 pm/°C
[10]	Misaligned HCF FPI	No	9.22 pm/°C
[15]	Gold coated SPR	No	−2.85 nm/°C
[17]	Liquid filled PCF-SPR	No	2.7 nm/°C
[16]	Gold film-SPR	No	−0.919 nm/°C
[21]	FBGs	No	10–13 pm/°C
[22]	LPFGs by Femtosecond	No	25.13 pm/°C
[28]	PCF liquid infiltration	No	6.3 pm/°C
[2]	Tapered multicore fiber	No	28.89 pm/°C
[12]	NOA65 based single FPI	No	2.2 nm/°C
[30]	Simplified HCF-FPI	Yes	1.019 nm/°C
[31]	Cascaded cavities of FPIs	No	10.45 pm/°C
[32]	Cascaded Sagnac	Yes	−13.36 nm/°C
[33]	Cascaded Sagnac Loops	Yes	11.4 nm/°C
[35]	Dual In-Line MZI	Yes	528.5 pm/°C
[36]	MZI with Vernier effect	Yes	397.36 pm/°C
[34]	Sagnac with FPI	Yes	−29 nm/°C
[37]	Hybrid MI and FPI	Yes	710 pm/°C
This paper	Dual cascaded FPIs (NOA65 + HCF)	Yes	67.693 nm/°C

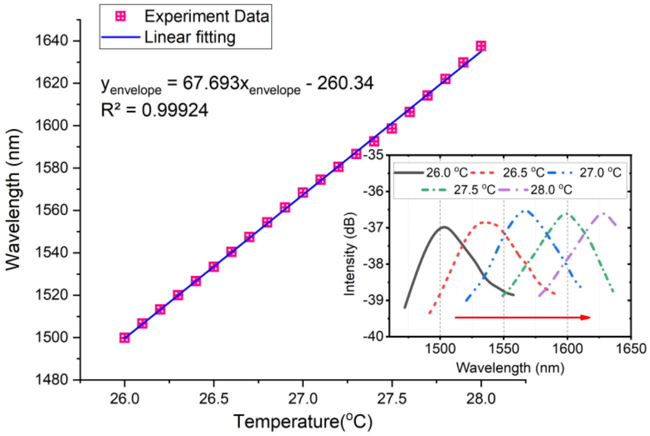

Figure 9. Sensitivity and linear correlation response of temperature sensor with dual cascaded FPIs, and the inset shows the spectral evolution of interference fringe shift with temperature rise.

4. CONCLUSION

A novel temperature sensor is proposed and experimentally demonstrated, which is composed of dual cascaded FPIs. The proposed architecture is fully capable of generating an efficient Vernier-effect. Dual in-fibre cavities are constituted with NOA65 thermo-sensitive polymer (FPIsensing) and HCF (FPIreference), which are formed in cascades. This device makes ultra-low temperature detection possible with a high resolution of 2.85×10^{-4}°C. Experimental results show that the proposed sensor produces an ultra-high sensitivity of 67.693 nm/°C with a high linear correlation, which is 20× times higher than that of a single FPI and consistent with theoretical analysis. Reference FPI possesses ultra-low sensitivity of 0.98 pm/°C and does not need to be isolated; therefore, it can be combined with sensing FPI to form a tiny temperature device for various practical applications.

REFERENCES

1. Mumtaz, F., et al., "A design of taper-like etched multicore fiber refractive index-insensitive a temperature highly sensitive Mach-Zehnder interferometer," *IEEE Sensors Journal*, Vol. 20, No. 13, 7074–7081, 2020.
2. Cheng, P., et al., "Refractive index interferometer based on SMF-MMF-TMCF-SMF structure with low temperature sensitivity," *Optical Fiber Technology*, Vol. 57, 102233, 2020.
3. Mumtaz, F., Y. Dai, and M. A. Ashraf, "Inter-cross de-modulated refractive index and temperature sensor by an etched Multi-core fiber of a MZI structure," *Journal of Lightwave Technology*, Vol. 38, No. 24, 6948–6953, 2020.
4. Mumtaz, F., H. Lin, Y. Dai, W. Hu, M. A. Ashraf, L. G. Abbas, S. Cheng, and P. Cheng, "Simultaneous measurement of temperature and strain using multi-core fiber within-line cascaded symmetrical ellipsoidal fiber balls-based Mach-Zehnder interferometer structure," *Progress In Electromagnetics Research C*, Vol. 112, 21–34, 2021.
5. Frazão, O., et al., "Simultaneous measurement of multiparameters using a Sagnac interferometer with polarization maintaining side-hole fiber," *Applied Optics*, Vol. 47, No. 27, 4841–4848, 2008.
6. Bai, Y., Y. Miao, H. Zhang, and J. Yao, "Simultaneous measurement of temperature and relative humidity based on a microfiber sagnac loop and MoS_2," *Journal of Lightwave Technology*, Vol. 38, No. 4, 840–845, 2020.
7. Cao, Y., H. Zhang, Y. Miao, Z. Ma, and B. Li, "Simultaneous measurement of temperature and refractive index based on microfiber Bragg Grating in Sagnac loop," *Optical Fiber Technology*, Vol. 47, 147–151, 2019.
8. Wang, G., Y. Lu, X. Yang, L. Duan, and J. Yao, "Square-lattice alcohol-filled photonic crystal fiber temperature sensor based on a Sagnac interferometer," *Applied Optics*, Vol. 58, No. 8, 2132–2136, 2019.
9. Liu, Y., et al., "Fabrication of dual-parameter fiber-optic sensor by cascading FBG with FPI for simultaneous measurement of temperature and gas pressure," *Optics Communications*, Vol. 443, 166–171, 2019.
10. Liu, Y., et al., "Hollow-core fiber-based all-fiber FPI sensor for simultaneous measurement of air pressure and temperature," *IEEE Sensors Journal*, Vol. 19, No. 23, 11236–11241, 2019.
11. Nan, J., D. Zhang, X. Wen, M. Li, H. Lv, and K. Su, "Elimination of thermal strain interference in mechanical strain measurement at high temperature using an EFPI-RFBG hybrid sensor with unlimited cavity length," *IEEE Sensors Journal*, Vol. 20, No. 10, 5270–5276, 2020.
12. Abbas, L. G., F. Mumtaz, Y. Dai, A. Zhou, W. Hu, and M. A. Ashraf, "Highly sensitive polymer based Fabry-Perot interferometer for temperature sensing," *Progress In Electromagnetics Research Letters*, Vol. 97, 87–94, 2021.
13. Del Carmen Alonso-Murias, M., J. S. Velázquez-González, and D. Monzón-Hernández, "SPR fiber tip sensor for the simultaneous measurement of refractive index, temperature, and level of a liquid," *Journal of Lightwave Technology*, Vol. 37, No. 18, 4808–4814, 2019.

14. Han, B., et al., "Simultaneous measurement of temperature and strain based on dual SPR effect in PCF," *Optics Laser Technology*, Vol. 113, 46–51, 2019.
15. Velázquez-González, J. S., D. Monzón-Hernández, D. Moreno-Hernández, F. Martínez-Piñón, and I. Hernández-Romano, "Simultaneous measurement of refractive index and temperature using a SPR-based fiber optic sensor," *Sensors Actuators B: Chemical*, Vol. 242, 912–920, 2017.
16. Zhang, R., S. Pu, and X. Li, "Gold-film-thickness dependent SPR refractive index and temperature sensing with hetero-core optical fiber structure," *Sensors*, Vol. 19, No. 19, 4345, 2019.
17. Lu, Y., M. Wang, C. Hao, Z. Zhao, and J. Yao, "Temperature sensing using photonic crystal fiber filled with silver nanowires and liquid," *IEEE Photonics Journal*, Vol. 6, No. 3, 1–7, 2014.
18. Xu, H., M. Hafezi, J. Fan, J. M. Taylor, G. F. Strouse, and Z. Ahmed, "Ultra-sensitive chip-based photonic temperature sensor using ring resonator structures," *Optics Express*, Vol. 22, No. 3, 3098–3104, 2014.
19. Yu, J., S. Xu, Y. Jiang, H. Chen, and W. Feng, "Multi-parameter sensor based on the fiber Bragg grating combined with triangular-lattice four-core fiber," *Optik*, Vol. 208, 164094, 2020.
20. Yan, L. S., A. Yi, W. Pan, and B. Luo, "A simple demodulation method for FBG temperature sensors using a narrow band wavelength tunable DFB laser," *IEEE Photonics Technology Letters*, Vol. 22, No. 18, 1391–1393, 2010.
21. Rao, Y.-J., "In-fibre Bragg grating sensors," *Measurement Science Technology*, Vol. 8, No. 4, 355, 1997.
22. Zheng, Z.-M., Y.-S. Yu, X.-Y. Zhang, Q. Guo, and H.-B. Sun, "Femtosecond laser inscribed small-period long-period fiber gratings with dual-parameter sensing," *IEEE Sensors Journal*, Vol. 18, No. 3, 1100–1103, 2017.
23. Cao, X., D. Tian, Y. Liu, L. Zhang, and T. Wang, "Sensing characteristics of helical long-period gratings written in the double-clad fiber by CO_2 laser," *IEEE Sensors Journal*, Vol. 18, No. 18, 7481–7485, 2018.
24. Zhang, A. P., L.-Y. Shao, J.-F. Ding, and S. L. He, "Sandwiched long-period gratings for simultaneous measurement of refractive index and temperature," *IEEE Photonics Technology Letters*, Vol. 17, No. 11, 2397–2399, 2005.
25. Zhou, J., et al., "Simultaneous measurement of strain and temperature by employing fiber Mach-Zehnder interferometer," *Optics Express*, Vol. 22, No. 2, 1680–1686, 2014.
26. Jiang, L., J. Yang, S. Wang, B. Li, and M. Wang, "Fiber Mach-Zehnder interferometer based on microcavities for high-temperature sensing with high sensitivity," *Optics Letters*, Vol. 36, No. 19, 3753–3755, 2011.
27. Alawsi, S. M. K. and M. A. Jabbar, "Refractive index and temperature sensor using HC-1550 infiltrating by different liquid crystal," *Optics Photonics Journal*, Vol. 8, No. 3, 29–39, 2018.
28. Zhou, Y., et al., "Simultaneous measurement of curvature and temperature based on PCF-based interferometer and fiber Bragg grating," *Optics Communications*, Vol. 284, No. 24, 5669–5672, 2011.
29. Wang, F., K. Pang, T. Ma, X. Wang, Y. J. O. Liu, and L. Technology, "Folded-tapered multimode-no-core fiber sensor for simultaneous measurement of refractive index and temperature," *Optics Laser Technology*, Vol. 130, 106333, 2020.
30. Zhang, P., et al., "Simplified hollow-core fiber-based Fabry-Perot interferometer with modified Vernier effect for highly sensitive high-temperature measurement," *IEEE Photonics Journal*, Vol. 7, No. 1, 1–10, 2015.
31. Tian, J., Y. Jiao, S. Ji, X. Dong, and Y. Yao, "Cascaded-cavity Fabry-Perot interferometer for simultaneous measurement of temperature and strain with cross-sensitivity compensation," *Optics Communications*, Vol. 412, 121–126, 2018.
32. Shao, L.-Y., et al., "Sensitivity-enhanced temperature sensor with cascaded fiber optic Sagnac interferometers based on Vernier-effect," *Optics Communications*, Vol. 336, 73–76, 2015.

33. Wang, G., B. Liao, Y. Cao, X. Feng, B.-O. Guan, and J. Yao, "Microwave photonic interrogation of a high-speed and high-resolution temperature sensor based on cascaded fiber-optic sagnac loops," *Journal of Lightwave Technology*, Vol. PP, No. 99, 1–1, 2020.
34. Yang, Y., et al., "Sensitivity-enhanced temperature sensor by hybrid cascaded configuration of a Sagnac loop and a FP cavity," *Optics Express*, Vol. 25, No. 26, 33290–33296, 2017.
35. Wang, Z., L. Huang, C. Liu, H. Wang, S. Sun, and D. Yang, "Sensitivity-enhanced fiber temperature sensor based on vernier effect and dual in-line mach-zehnder interferometers," *IEEE Sensors Journal*, Vol. 19, No. 18, 7983–7987, 2019.
36. Liao, H., et al., "Sensitivity amplification of fiber-optic in-line Mach-Zehnder Interferometer sensors with modified Vernier-effect," *Optics Express*, Vol. 25, No. 22, 26898–26909, 2017.
37. Abbas, L. G. and H. Li, "Temperature sensing by hybrid interferometer based on Vernier like effect," *Optical Fiber Technology*, Vol. 64, 102538, 2021.
38. Tan, X., Y. Geng, X. Li, Y. Deng, Z. Yin, and R. Gao, "UV-curable polymer microhemisphere-based fiber-optic Fabry-Perot interferometer for simultaneous measurement of refractive index and temperature," *IEEE Photonics Journal*, Vol. 6, No. 4, 1–8, 2014.
39. Cao, K., Y. Liu, and S. Qu, "Compact fiber biocompatible temperature sensor based on a hermetically-sealed liquid-filling structure," *Optics Express*, Vol. 25, No. 24, 29597–29604, 2017.